ELSEVIER

Catalysis Today 39 (1997) 45–59

CATALYSIS TODAY

# Preparation and characterization of zeolite-supported molybdenum and cobalt–molybdenum sulfide catalysts

Yasuaki Okamoto*

*Department of Materials Science, Shimane University, Matsue 690, Japan*

**Abstract**

Preparation, characterization and catalysis of zeolite-supported Mo, Co(Ni) and Co(Ni)–Mo sulfide catalysts have been reviewed in the present article. Incomplete sulfidation of Mo oxides and poor dispersion of Mo sulfides were observed for zeolite-supported Mo catalysts prepared by impregnation methods, accompanied by a considerable crystallinity loss at a high calcination temperature. A significant migration of Mo oxide species into zeolite pores was noted during the calcination, producing Mo oxo-species in tetrahedral coordinations. Incorporation of Mo into zeolite using ion-exchange techniques and solid–solid reactions is briefly described. Metal carbonyl techniques provided highly dispersed and fully sulfided intrazeolite Mo and Co sulfide clusters by use of $Mo(CO)_6$ and $Co(CO)_3NO$, respectively. The Mo sulfide catalysts encaged in NaY exhibited much higher HDS activities than the impregnation catalysts. Co–Mo binary sulfide clusters were successfully synthesized in the pores of NaY as evidenced by EXAFS and XPS. The Co sites of the clusters were found to play important roles in hydrogenation and HDS. Thermally stable and catalytically active binary sulfide clusters for HDS are proposed to be intrazeolite $Co_2Mo_2S_6$ molecular clusters. It was demonstrated that catalytic synergy between Co and Mo sulfides was generated by Co–S–Mo chemical bond formations. © 1997 Elsevier Science B.V.

*Keywords:* Hydrodesulfurization; Mo sulfide catalysts; Co sulfide catalysts

## 1. Introduction

Hydrocracking of petroleum feedstocks, in particular of heavy residues, is of growing importance for more efficient utilization of natural resources. The configuration of hydrocracking processes [1] is classified into (i) two-stage hydrocracker where hetero-atom removal and hydrocracking reactor-stages are separated with inter-stage product removal; (ii) series-flow hydrocracker where the two reactor-stages are in series without inter-stage product removal and (iii) single-stage hydrocracker consisting of a single reactor to perform multi-functions of hetero-atom removal, hydrogenation and hydrocracking. In the last two configurations, hydrocracking reactions occur in the presence of $H_2S$ and $NH_3$, which are the products of the preceding or simultaneous hydrodesulfurization and hydrodenitrogenation reactions, respectively. This type of hydrocracking is only possible with the use of zeolites, which have sufficient $NH_3$ resistance, combined with the catalytic components possessing hydrogenation activities. For the latter purposes, metal sulfides are excellent candidates for hydrogenation in the presence of $H_2S$.

Zeolite-supported Mo and Co(Ni)–Mo sulfide catalysts have recently received much attention as a promising type of hydrocracking catalysts in petro-

*Corresponding author. Tel.: 0852-32-6466; fax: 0852-32-6429; E-mail: yokamoto@riko.shimane-u.ac.jp


*PII* S0920-5861(97)00087-4

leum industries [1–3]. Both the cracking activity of the zeolite and the hydrogenation and hetero-atom removal activities of the metal sulfide phases are required to be finely controlled for higher performances, depending on petroleum feedstocks and desired selectivity: e.g., naphtha, kerosene or gas–oil mode. Preparation of zeolite-supported, highly dispersed metal sulfides is considered to be one of the most important factors for these purposes. In the present review, I focused my attention on zeolite-supported Mo and Co(Ni)–Mo sulfide systems, in particular, on our studies on the preparation, characterization and catalytic properties of highly dispersed Mo and Co–Mo sulfides encaged in zeolite by use of metal carbonyls.

## 2. Incorporation of active species in zeolite

### 2.1. Oxidic states

Many fundamental researches have been conducted on Mo catalysts supported on zeolite in both oxidic and sulfided states. The most conventional method to support Mo is an impregnation technique using aqueous solutions of ammonium heptamolybdate, followed by drying and subsequent calcination. The chemical state, dispersion and location of zeolite-supported Mo oxide or sulfide species prepared by impregnation methods depend on the Mo loading and calcination temperature.

Lopez Agudo et al. [4] studied the effects of calcination temperature on the crystallinity and thiophene conversion with $MoO_3$/NaY and $MoO_3$/$NH_4$Y (10 wt% $MoO_3$). It was found by means of XRD and sorption capacity that a significant loss of crystallinity of the host zeolite was observed at a calcination temperature higher than 623 K. The activity of $MoO_3$/NaY decreased as the calcination temperature increased between 623 and 773 K; this was ascribed to decreasing dispersions of accessible active Mo phases as a result of the crystallinity loss. On the other hand, the HDS activity of $MoO_3$/$NH_4$Y increased with increasing calcination temperature. It was suggested that the increase in acidity due to a decomposition of $NH_4^+$ caused the increase in the activity of $MoO_3$/$NH_4$Y. Many workers [5–8] reported similar destruction of NaY and HY zeolite structures upon calcination at 773–793 K. According to Cid et al. [5], the extent of crystallinity loss of NaY increased as the Mo content increased. The decreases of both surface area and water adsorption capacity resulted from this loss. The presence of Co was found to stabilize the zeolite structure upon Mo introduction [6]. In the case of USY zeolite, however, no crystallinity loss was reported to take place [9]. With $MoO_3$/H-ZSM-5 prepared by an impregnation technique, Lopez Agudo et al. [10] found that the zeolite crystallinity was mostly preserved at 6 wt% $MoO_3$ and that most of Mo species were present on the external surface as crystalline $MoO_3$.

Impregnation of an aqueous ammonium heptamolybdate solution on zeolite is expected to cause surface agglomeration of anionic Mo species on the external surface of the zeolite particles, since zeolite has no anion-exchanging properties. During calcination, penetrations of the Mo species into the zeolite cages were evidenced by FTIR studies of the surface OH groups [11] and zeolite framework vibrations [5], pore volume measurements [9], XPS [7,11] and $^{129}$Xe NMR [8]. The migration of Mo species into zeolite was found to result in the formation of Mo oxide species in tetrahedral coordinations. The FTIR studies of $MoO_3$/NaY [5,7] and $MoO_3$/USY [9] showed a band around 890–900 $cm^{-1}$ characteristic to $MoO_4^{2-}$ species, consistent with the results by diffuse reflectance spectra [5]. Very recently, by means of X-ray absorption near edge structure (XANES) of Mo K-edge shown in Fig. 1, Okamoto and Katsuyama [12] have demonstrated that a majority of Mo oxide species are in tetrahedral configurations on $MoO_3$/NaY (5 and 14.5 wt% Mo) calcined at 773 K. In conformity with the formation of tetrahedral Mo oxide species encaged in zeolite, only a part of Mo species was extracted by aqueous $NH_3$ solutions; e.g., 60% or more of Mo was retained in zeolite with $MoO_3$/NaY [5] and CoO–$MoO_3$/NaY [6].

At a relatively low calcination temperature (<673 K), the migration of Mo oxide species is limited. In their systematic study on a series of $MoO_3$/NaY having 3.5–10.4 wt% Mo, Vorbeck et al. [13] suggested on the basis of $^{129}$Xe NMR that only a part of Mo was located inside the pores (ca. 25%) with a majority of the Mo species being on the external surface of the zeolite. When a mixture of $MoO_3$ and zeolite was heated for 24 h in the presence of

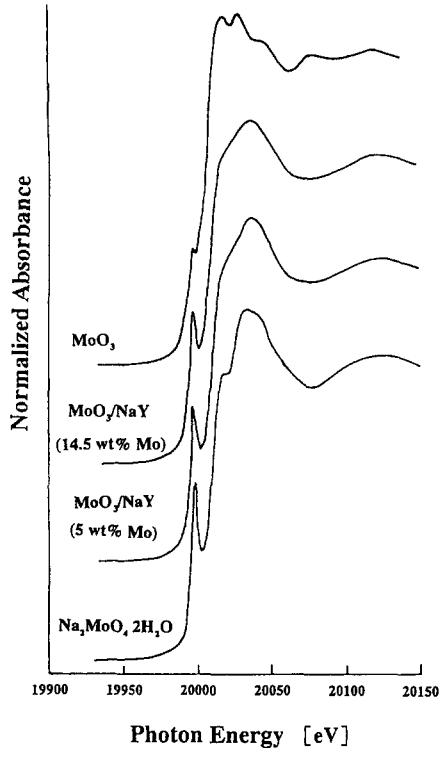


Fig. 1. Normalized Mo K-edge XANES spectra for $Na_2MoO_4 \cdot 2H_2O$, $MoO_3$/NaY (5 wt% Mo), $MoO_3$/NaY (14.5 wt% Mo) and $MoO_3$.

$H_2O$ vapor, no reaction was observed to occur at <600 K [8]. However, between 680 and 750 K, migration of Mo oxide species into zeolite was observed by means of Xe adsorption and $^{129}Xe$ NMR. The mechanism of the Mo penetration has been proposed as follows [7]:

$$MoO_3 + H_2O \rightarrow MoO_2(OH)_2 \quad (1)$$

The formation of $MoO_2(OH)_2$ with a relatively high vapor pressure results in a high mobility of Mo species. The productions of Mo species in tetrahedral coordinations are in good agreement with the proposed mechanism.

Heat-treatments of a physical mixture of $MoO_3$ and zeolite cause a migration of Mo species into zeolite cages [8,14] as shown above. Recently, this technique was successfully applied to the introduction of dispersed Mo oxides into SAPO-5 [15] and mesoporous materials, MCM-41 [16,17]. By use of an incipient wetness impregnation technique, no destruction of pore structure of MCM-41 was reported for NiO–$MoO_3$/MCM-41 (12 wt% $MoO_3$ and 3 wt% NiO) calcined at 773 K [18].

Incorporation of Mo species into zeolite pores is also conducted by ion-exchange techniques using $MoO_2Cl_2$ [19–21]. Minming and Howe [20] reported a retention of crystallinity of NaY during ion-exchanging. An FTIR study suggested a formation of oxomolybdenum species, $MoO_2(H_2O)^{2+}$, in the presence of $H_2O$. It was very hard for the Mo species to be reduced by $H_2$; a maximum of 18% of $Mo^{6+}$ was reduced to $Mo^{5+}$ at >570 K. They proposed a migration of Mo species into β-cages or double hexagonal rings (D6R).

$MoCl_5$ can be used to introduce Mo into acidic zeolite cages by a solid–solid exchange [9,22–25]. In this case, reactions of $MoCl_5$ or $MoOCl_4$ with zeolitic hydroxyl groups are involved to anchor Mo species, producing HCl. ESR, XRD, XPS and FTIR results confirmed that Mo ions were indeed exchanged into zeolite with some loss in crystallinity [22]. $(Mo^{6+}{=}O)^{4+}$ and $(Mo^{6+}{-}OH)^{5+}$ complex ions were postulated to be located as SII sites. The Mo species thus prepared in zeolite were shown to exhibit an activity for epoxidation of cyclohexene using *t*-$BuO_2H$ and $O_2$ [23]. $MoCl_5$ was also employed to introduce Mo into aluminophosphate pores ($ALPO_4$-5) [26].

Adsorption of $Mo(CO)_6$ into zeolite cages from a vapor phase or from a solution has been recently employed to prepare zeolite-supported Mo metal, oxide or sulfide catalysts [27,28]. In the case of Y-type zeolite, two molecules of $Mo(CO)_6$ can be accommodated in a supercage at saturation [27–29]. The transformation of $Mo(CO)_6$ encaged in zeolite to Mo sulfide hydrotreating catalysts has been conducted by (i) direct sulfidation [13,30,31], (ii) sulfidation after a partial decomposition of $Mo(CO)_6$ to subcarbonyl species [13,30,32,33], (iii) sulfidation after a complete decomposition to metallic Mo [13,34] or (iv) sulfidation after an oxidation to Mo oxide species [9,12,13,35]. The structure of Mo oxide species prepared by a mild photo- or thermal-oxidation of $Mo(CO)_6$ encaged in NaY was studied using extended X-ray absorption fine structure (EXAFS) techniques. Jelinek et al. [36] proposed a monomeric $Mo^{6+}$ oxide species, while Okamoto et al. [37] proposed a dimer species encaged in zeolite pores. The difference may

be ascribed to the oxidation conditions. On the basis of ESR results on Mo/HY prepared using $Mo(CO)_6$ and calcined at >600 K, Abdo and Howe [38] showed $Mo^{5+}$ species to be in β-cages or D6R sites of the zeolite.

Ni or Co ions are usually introduced into zeolite by ion-exchange procedures or impregnation techniques. Mo and Co(Ni) component species are supported separately or simultaneously. Co carbonyls are also used for zeolite-supported Co catalysts. Howe et al. [26] used $Co(CO)_3NO$ adsorbed on NaY as a precursor of CO hydrogenation catalysts. Two molecules of $Co(CO)_3NO$ were incorporated at the same time in the supercage of NaY [39]. Very recently, $Co_2(CO)_8$ was employed to introduce Co species into NaY zeolite [40]. These materials would be good candidates of highly dispersed Co sulfides encaged in zeolite.

### 2.2. *Sulfided states*

The characterization of zeolite-supported metal sulfide catalysts has been conducted to a much less extent than that of oxidic catalysts. Many workers showed incomplete sulfidation of Mo oxides/zeolite prepared by impregnation techniques [21,41,42]; a S/Mo atomic ratio was usually around 1 or less when $MoO_3$/zeolite was calcined at >770 K prior to sulfidation. Figs. 2 and 3 illustrate the EXAFS [12,43] and XPS [43] results on $MoO_3$/NaY sulfided at 673 K. The Fourier transform of sulfided $MoO_3$/NaY ($MoS_2$/NaY) shows the presence of Mo–O bondings as well as Mo–S and Mo–Mo bondings due to crystalline $MoS_2$. The structural parameters obtained from the EXAFS results are summarized in Table 1. The Mo3d XPS spectrum for $MoS_2$/NaY indicates that $Mo^{5+}$ and $Mo^{6+}$ oxide and/or oxysulfide species are present after sulfidation for 5 h at 673 K. These results obviously demonstrate a partial sulfidation of Mo oxide species in $MoO_3$/NaY (5 wt% Mo) calcined at 773 K. Incomplete sulfidation of impregnation catalysts is ascribed to the formations of isolated tetrahedrally coordinated Mo oxide species as exemplified in Fig. 1. These Mo oxide species are deduced to strongly interact with zeolite frameworks [4,11] and/or to locate in β-cages or D6R sites [20,38].

Vorbeck et al. [13] studied the degree of sulfidation of $MoO_3$/NaY calcined at a lower temperature, 673 K,

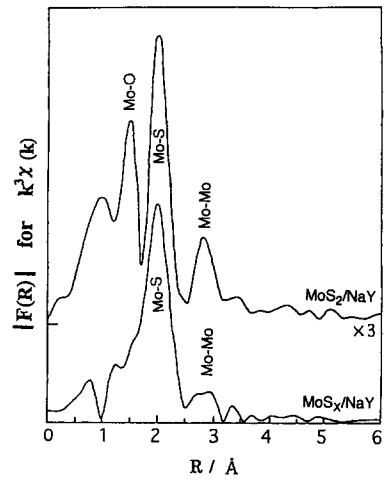


Fig. 2. Fourier transforms of $k^3$-weighted EXAFS modulations of the Mo K-edge for $MoS_2$/NaY (5 wt% Mo or 0.8Mo/SC) sulfided at 673 K for 5 h and MoSx/NaY (12 wt% Mo or 2Mo/SC) sulfided at 673 K for 1.5 h.

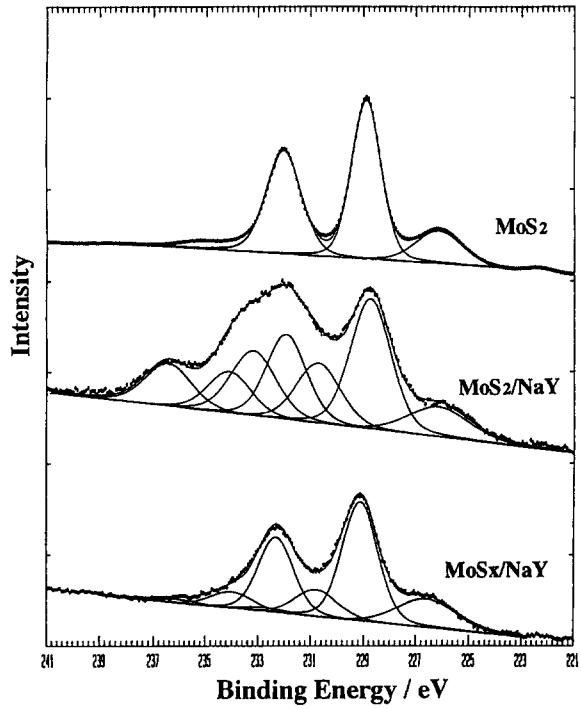


Fig. 3. XP spectra of the Mo3d level for MoSx/NaY (2.1Mo/SC), $MoS_2$/NaY (14.5 wt% Mo or 2.4Mo/SC) and polycrystalline $MoS_2$.

as a function of the Mo loading. The S/Mo atomic ratio was found to decrease as the Mo content increased (S/Mo =2.2 for 3.5 wt% Mo to 1.3 for 10.4 wt% Mo).

Table 1
Structural parameters[a] as derived from the Mo K-edge EXAFS for Mo, Co–Mo and Fe–Mo sulfide catalysts encaged in a NaY zeolite

| Catalyst | Loading/SC[b] | | Bondings | $R$ (Å) | CN | $E_0$ (eV) | $\Delta\sigma^2$ (Å$^2$) |
|---|---|---|---|---|---|---|---|
| | Mo | Co or Fe | | | | | |
| MoSx/NaY[c] | 2.1 | — | Mo-S | 2.40 | 4.7 | −2.3 | 0.0048 |
| | | | Mo-Mo | 3.15 | 1.1 | −2.0 | 0.0089 |
| $MoS_2$/NaY[d] | 0.8 | — | Mo-O | 1.78 | 0.8 | 12.7 | 0.0017 |
| | | | Mo-S | 2.42 | 1.1 | −5.0 | 0.0016 |
| | | | Mo-Mo | 3.16 | 1.2 | −3.8 | 0.0110 |
| CoSx–Mo–Sx/NaY | 2.1 | 2.1 | Mo-S | 2.41 | 5.0 | −5.8 | 0.0020 |
| | | | Mo-Mo | 3.18 | 0.7 | 0.2 | 0.0079 |
| | | | Mo-Co[e] | 2.83 | — | — | — |
| FeSx–MoSx/NaY | 2.0 | 1.8 | Mo-S | 2.39 | 4.8 | −5.5 | 0.0052 |
| | | | Mo-Mo | 3.17 | 0.9 | −2.2 | 0.0056 |

[a] $R$, Bond distance; CN, coordination number; $E_0$, inner potential; $\sigma$, Debye–Waller-like factor.
[b] Metal atoms/superage.
[c] Sulfided at 673 K for 1.5 h.
[d] 5 h.
[e] Bond distance was estimated using theoretical parameters.

It was suggested that higher loadings caused larger $MoO_3$ particles which were more difficult to sulfide down to their core. A complete sulfidation of Mo was reported by Lopez Agudo et al. [10] for H-ZSM-5-supported $MoO_3$ catalysts calcined at 773 K. This may suggest a formation of well dispersed $MoO_3$ on the external surface of H-ZSM-5 at the calcination temperature.

The degrees of sulfidation, S/Mo, of $MoO_2^{2+}$ ion-exchanged HY calcined at 773 K [21] and of $Mo(CO)_6$-derived Mo oxide/USY calcined at 723 K [42] were also considerably lower than the two for a complete sulfidation of Mo. On the other hand, a direct sulfidation of $Mo(CO)_6$ or Mo subcarbonyl species resulted in a complete sulfidation of Mo [12,13,43]. In conformity with the above results, Laniecki and Zmierczak [32] observed $Mo^{5+}$ ESR signals with $MoO_3$/NaY or HNaY after sulfidation at 675 K, whereas they detected no signals with $Mo(CO)_6$-derived catalysts. The EXAFS results in Fig. 2 and Table 1 indicate the formation of Mo–S and Mo–Mo bondings for a Mo sulfide catalyst prepared by a direct sulfidation of $Mo(CO)_6$/NaY (MoSx/NaY). The XPS results in Fig. 3 corroborate a complete sulfidation of Mo in MoSx/NaY.

The thiophene HDS activities of zeolite-supported Mo sulfide catalysts prepared by $Mo(CO)_6$-adsorption and Mo anion-impregnation methods are compared in Table 2 [31]. Obviously, the $Mo(CO)_6$-derived MoSx/zeolite catalysts showed considerably higher activities than the impregnation catalyst. It was demonstrated by an NO adsorption technique that the higher activity was due to a higher dispersion of Mo sulfide species in MoSx/zeolite [31]. It was found in Table 2 that the specific activity per Mo depended on the host zeolite. Laniecki and Zmierczak [32] reported that $Mo(CO)_6$-derived Mo/NaY catalysts showed higher activities for thiophene HDS and water gas shift reactions as compared to impregnation catalysts. They attributed the findings to higher dispersions of Mo sulfide species in the former catalysts on the basis of NO adsorptions.

Table 2
Catalytic activities of zeolite-supported Mo sulfide catalysts, which were prepared by use of $Mo(CO)_6$ as a precusor, for hydrodesulfurization of thiophene at 673 K

| Zeolite | Mo loading (wt% Mo) | HDS activity (% conv./ g-Mo) |
|---|---|---|
| HY | 9.4 | 48 |
| LiY | 12 | 136 |
| NaY | 12 | 176 |
| NaY[a] | 4.8 | 60 |
| KY | 10 | 205 |
| RbY | 9.3 | 134 |
| CsY | 8.7 | 128 |

[a] Prepared by impregnation, followed by calcination at 773 K.

The sulfidation behaviors and catalytic properties of Ni and Co supported on zeolite have been examined to

an even less extent. Leglise et al. [41] found a complete sulfidation of Ni at 593 K to $Ni_3S_2$ and, probably, NiS with Ni/USY and Ni–Mo/USY. The benzene hydrogenation activity of a supported Ni–Mo sulfide catalyst at 440 K decreased in the order: Ni–Mo/$Al_2O_3$>Ni–Mo/USY>Mo/USY>Ni/USY. The turnover frequency of Ni–Mo/USY defined by $O_2$ chemisorption was close to that of the $Al_2O_3$-supported counterpart, suggesting a Ni–Mo–S phase formation in Ni–Mo/USY catalysts. An FTIR study of CO adsorption (2086 $cm^{-1}$) corroborated the formation of a Ni–Mo–S phase, as proposed for Ni–Mo/$Al_2O_3$ (2079 $cm^{-1}$). An XPS study by Ezzamarty et al. [21] showed that with Ni/USY and Ni–Mo/USY, the dispersion of Ni increased by sulfidation or by a combination with Mo.

According to Welters et al. [44], chemical analysis as well as temperature programmed sulfidation measurements showed a complete sulfidation of Ni on ion-exchanged Ni/NaY catalysts. The Ni sulfide phase consisted mainly of $Ni_3S_2$, probably accompanied by a small amount of NiS. The proportion of NiS depended on the extent of dehydration of Ni/NaY before sulfidation. High resolution electron microscopy (HREM) and $^{129}Xe$ NMR indicated that a major part of the Ni sulfide phase was invariably located on the outside of the zeolite particles. Small Ni sulfide clusters in the pores of the zeolite were suggested to exhibit very high activities for thiophene HDS. Ni/NaY catalysts prepared by ion-exchange showed much higher thiophene HDS activities than impregnation catalysts [13]. It was suggested that the activity difference was due to the large differences in Ni sulfide distribution and dispersion and to the acidic sites created during the sulfidation of the ion-exchanged catalysts.

Characterization of zeolite-supported Co–Mo sulfide catalysts was conducted by Cid et al. [6,45]. It was shown using XRD and FTIR that the decrease in crystallinity observed upon introduction of Mo into zeolite was much smaller in the presence of Co. The Co–Mo/NaY or HNaY catalysts prepared by ion-exchange of Co and subsequent impregnation of Mo exhibited higher activity for thiophene HDS than the catalysts prepared by simultaneous impregnation of Co and Mo. This was suggested to be associated with a poorer dispersion of Co in the latter catalysts, in which a fraction of Co was present as $Co_3O_4$. The ion-exchanged catalysts showed higher hydrocracking activity; this apparently can be ascribed to higher acidity generated by sulfidation of $Co^{2+}$ cations.

$$Co^{2+}(Oz)_2 + H_2S \rightleftarrows CoS + 2(Oz\text{-}H^+) \quad (2)$$

where Oz denotes framework oxygen. A reverse reaction of metal sulfide clusters with the resultant surface hydroxyl groups was observed to take place even at room temperature for CdS encaged in zeolite [46].

$$Cd^{2+}(Oz)_2 + H_2S \rightleftarrows CdS + 2(Oz\text{-}H^+) \quad (3)$$

CdS clusters were found to be stabilized only in the presence of $H_2S$.

Very recently, Taniguchi et al. [47] successfully employed an ion-exchange technique to introduce Mo and Ni–Mo composite sulfide clusters into zeolite cavities using $[Mo_3S_4(H_2O)_9]^{4+}$ and $[Mo_3NiS_4Cl(H_2O)_9]^{3+}$, respectively, as precursors. The benzothiophene HDS activity was found to be significantly affected by the zeolite structure. Mo/K-LTL and Mo/Na–MOR catalysts exhibited superior activity to Mo/NaY, Mo/USY or Mo/NaH-β.

The dispersion, location and sulfidation behaviors of active metal sulfide species have rarely been investigated up to now with zeolite-supported Co(Ni)–Mo catalysts.

## 3. Molybdenum and cobalt sulfides encaged in zeolite using metal carbonyls

Metal carbonyls have been employed as precursors to prepare highly dispersed metal sulfide clusters supported on $Al_2O_3$ [48–50] or encaged in zeolite [12,31,50]. Vrinat et al. [34] employed, for the first time, $Mo(CO)_6$ to prepare Mo sulfide catalysts supported on NaY, HY and their Co-exchanged forms for the HDS of benzothiophene. However, the sulfide catalysts thus prepared showed only low HDS activities. The catalysts were prepared by decomposing $Mo(CO)_6$ in zeolites at 600 K prior to the HDS reaction. The observed low activity apparently results from a low dispersion of Mo metal at the decomposition temperature. In our study [12,31,39,43,50], $Mo(CO)_6$ encaged in zeolite was directly and cautiously sulfided in situ in a stream of $H_2S/H_2$ (1/9) at 673 K. High chemical reactivities of Mo subcarbonyl species [28,31,51] produced during heat-treatments lead to

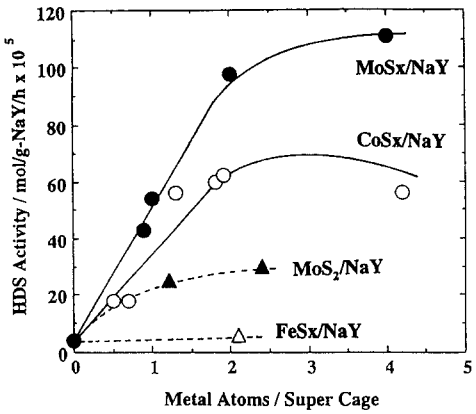


Fig. 4. Catalytic activities of MoSx/NaY (●), CoSx/NaY (○), $MoS_2$/NaY (▲) and FeSx/NaY (△) for the HDS of thiophene at 623 K as a function of the metal content (metal atoms/SC).

a complete sulfidation of Mo at a low temperature (300–400 K) [12,31].

The catalytic activities of NaY-supported Mo sulfide catalysts prepared using $Mo(CO)_6$ adsorption (MoSx/NaY) and impregnation ($MoS_2$/NaY) techniques are compared in Fig. 4 as a function of the Mo loading [39,52]. As aforementioned, MoSx/NaY exhibited a three or four times higher HDS activity than $MoS_2$/NaY. The activity of MoSx/NaY increased linearly with the Mo content up to 2Mo/supercage (SC), suggesting a formation of uniform Mo sulfide species in this concentration range [12,39,43]. The activity leveled off, however, at a further addition of Mo.

The structure, dispersion and sulfidation degree of the Mo sulfides supported on NaY zeolite were studied by EXAFS [12,43] and XPS [43]. The results are presented in Fig. 2 and Fig. 3, respectively, indicating a complete sulfidation of Mo species in MoSx/NaY. The structural parameters obtained from EXAFS are shown in Table 1 for MoSx/NaY (12.5 wt% Mo or 2.1Mo/SC). The Mo–Mo coordination number for MoSx/NaY was very close to unity and much smaller than the six for crystalline $MoS_2$ or, more precisely, the ratio of the coordination numbers of Mo–Mo and Mo–S bondings is 0.23 and much smaller than the unity for $MoS_2$. These findings suggest that the cluster size of the Mo sulfide species in MoSx/NaY is significantly small, in conformity with a high NO adsorption capacity [31,32]. The structure and dispersion of the Mo sulfides were not modified by a prolonged treatment (20 h) at 673 K in $H_2S/H_2$ [12]. Besides, the identical EXAFS parameters were obtained for a NaY-supported Mo sulfide catalyst prepared by sulfiding Mo oxide dimer species [37] fabricated by a mild oxidation of $Mo(CO)_6$/NaY. It is deduced that a specific Mo sulfide structure consisting of dimer units is formed in MoSx/NaY.

With $MoS_2$/NaY, on the other hand, incomplete sulfidation of Mo is concluded from the EXAFS and XPS results, as discussed above. The ratio of the coordination numbers of Mo–Mo and Mo–S bondings for $MoS_2$/NaY is close to unity. This suggests that the cluster size of Mo sulfide species is considerably large or that the dispersion of the Mo sulfide species is poor. A low NO adsorption capacity of $MoS_2$/NaY [31,32] is consistent with the low dispersion of the Mo sulfide species. The considerably higher HDS activities of MoSx/NaY in Table 2 and Fig. 4 are evidently attributed to a complete sulfidation of $Mo(CO)_6$ and a much higher dispersion of the resultant Mo sulfide species as compared to $MoS_2$/NaY.

The location, e.g., inside or outside the zeolite, of finely dispersed Mo sulfide species is of significant importance to catalyst performances for hydrocracking reactions [43]. Fig. 5 depicts the XRD patterns for NaY and MoSx/NaY [43,53]. A comparison of the patterns indicates no destruction of the structure of the host zeolite upon the introduction of the Mo sulfide species. In addition, the intensities of a few diffraction peaks such as 111 and 220 decreased on the accommodation of the Mo sulfides, while the intensity of 222 diffraction peak increased, showing that the electron

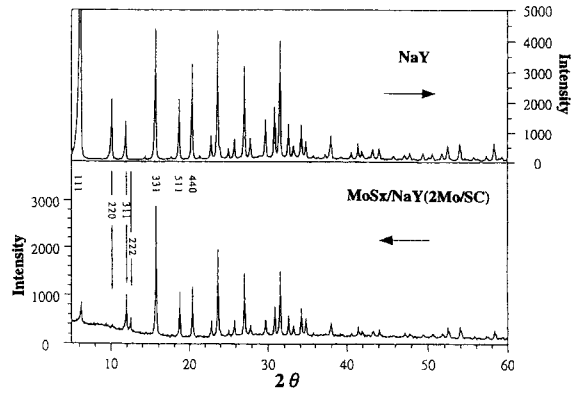


Fig. 5. X-ray powder diffraction patterns for NaY and MoSx/NaY (2.1Mo/SC).

Table 3
HDS reactions of substituted thiophenes on Mo sulfide catalysts supported on NaY and $Al_2O_3$

| Catalyst | Mo loading (wt%) | Activity [a] | | |
|---|---|---|---|---|
| | | TP | DMTP | TMTP |
| $MoS_2/Al_2O_3$ | 10.0 | 68.4 | 29.3 | 19.6 |
| | | (1.00) | (0.43) | (0.29) |
| MoSx/NaY | 14.5 | 97.5 | 35.0 | 13.8 |
| | | (1.00) | (0.36) | (0.14) |
| $MoS_2$/NaY | 14.5 | 30.0 | | 5.0 |
| | | | (1.00) | (0.17) |

[a](mol/g-support$\times 10^{-5}$).
The number in parentheses is the activity relative to TP.
TP: thiophene; DMTP: 2,5-dimethyl thiphene; TMTP: tetramethyl thiophene.

distribution is modified to possess antisymmetric character with respect to the centers of the supercages by the incorporation of the Mo sulfide clusters. This fact suggests that the Mo sulfide species are produced inside the zeolite pores.

The pore volumes of NaY and MoSx/NaY (2.1Mo/SC) were 0.298 and 0.235 $cm^3$ (g-zeolite)$^{-1}$, respectively, on the basis of benzene adsorption [43]. The volume occupied by the Mo sulfide species is estimated to be 0.043 $cm^3$ (g-zeolite)$^{-1}$, taking into consideration the density of $MoS_2$ and the Mo content. The observed decrease of 0.063 $cm^3$ (g-zeolite)$^{-1}$ for MoSx/NaY is even larger than the estimated value, indicating that a majority of the Mo sulfide species are accommodated in the host zeolite.

The location of Mo sulfide species in NaY zeolite was assessed by relative HDS rates of substituted thiophenes [43]. Table 3 compares the activities of NaY and $Al_2O_3$-supported Mo sulfide catalysts for the HDS of thiophene (TP), dimethylthiophene (DMTP) and tetramethylthiophene (TMTP). In the case of $MoS_2/Al_2O_3$ with an average pore diameter of 19–20 nm, the relative rate of the HDS of TMTP was 0.29 with respect to that of TP. The lower activity for the TMTP HDS reaction is due to a lower reactivity of TMTP as compared to that of TP [54,55]. MoSx/NaY prepared using $Mo(CO)_6$ showed a considerably reduced (0.14) relative activity for the HDS of TMTP compared to that of $MoS_2/Al_2O_3$. $MoS_2$/NaY also showed a similarly low relative activity. With DMTP, no strong molecular sieving effects were observed. These results indicate that a majority of the catalytically active Mo sulfide species in the zeolite-supported Mo sulfide catalysts are located in the zeolite cages [43]. This is in line with the suggestions by Vorbeck et al. [13]. The EXAFS, XRD, pore volume measurements and relative HDS activities demonstrate that highly dispersed Mo sulfide species are fabricated in NaY zeolite cages by use of $Mo(CO)_6$. HREM observations of MoSx/NaY (2Mo/SC) corroborated the above conclusions [43,53], indicating no destruction of the host zeolite crystal upon Mo sulfide incorporation and no agglomeration of Mo sulfide species on the external surface of the NaY zeolite. The high thermal stability of the Mo sulfide species is possibly owing to confinement effects in zeolite cages; diffusions and migrations of the Mo sulfide clusters are considered to be strongly suppressed by the molecular sized windows (0.74 nm) connecting supercages.

Fig. 4 shows that NaY-supported Co sulfide catalysts, CoSx/NaY, prepared using $Co(CO)_3NO$ exhibit considerably high activities for the HDS of thiophene, being comparable to those of MoSx/NaY [39,52]. The Fourier transforms of Co K-edge for CoSx/NaY (2Co/SC) and $Co_9S_8$ are compared in Fig. 6 [52]. Only a very small contribution of Co–Co bondings was observed for CoSx/NaY in contrast to that for $Co_9S_8$, substantiating a formation of extremely, highly dispersed Co sulfide clusters possibly in zeolite cages

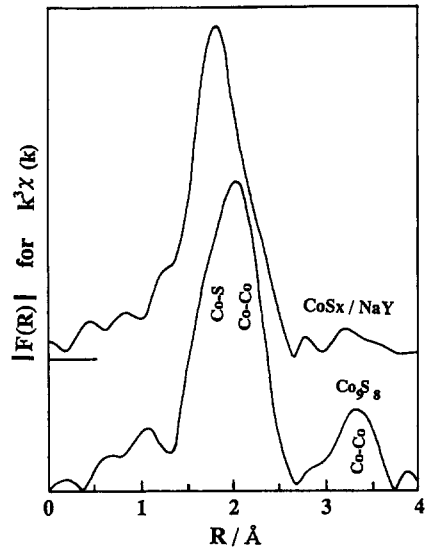


Fig. 6. $k^3$-weighted Fourier transforms of the Co K-edge EXAFS of CoSx/NaY (2Co/SC) and $Co_9S_8$.

as observed for the Mo sulfide clusters in MoSx/NaY. The high HDS activity of CoSx/NaY is considered to be attributed to the high dispersion of the Co sulfide species. Vissers et al. [56] proposed that high HDS activities of carbon-supported Co sulfide catalysts were due to extremely high dispersions of Co sulfide species over the support. FeSx/NaY prepared by use of $Fe(CO)_5$ as a precursor showed a negligible HDS activity at 623 K as illustrated in Fig. 4 [52].

## 4. Co–Mo binary sulfide catalysts encaged in zeolite

As demonstrated above, highly dispersed Mo and Co sulfide clusters are prepared in the zeolite pores using $Mo(CO)_6$ and $Co(CO)_3NO$ as precursors, respectively. Co–Mo binary sulfide species were fabricated by introducing $Co(CO)_3NO$ into MoSx/NaY or by admitting $Mo(CO)_6$ into CoSx/NaY, followed by a second sulfidation at 673 K. Fig. 7 shows the HDS activity of CoSx–MoSx/NaY (2.1Mo/SC) as a function of Co content [39]. CoSx–MoSx/NaY was prepared by $Co(CO)_3NO$ introduction to MoSx/NaY. The HDS activity increased as the Co/Mo ratio increased up to about unity, accompanied by an activity decrease at a further addition of Co. The observed activity of the mixed sulfide catalyst was considerably larger than the simple sum of the separate metal sulfide catalysts, indicating the generation of a catalytic synergy between the Co and Mo sulfides encaged in zeolite cavities. The activity of CoSx–MoSx/NaY was not changed by a treatment at 673 K in $H_2S/H_2$ for 20 h, demonstrating that the catalytically active species are thermally stable. The HDS activity of the Co–Mo binary sulfide catalyst was independent of the accommodation order of Mo and Co so long as the catalyst composition was the same [39].

The hydrogenation (HYD) of butadiene was conducted as a test reaction [39]. The HYD activity of MoSx/NaY was found to slightly decrease with increasing Co content up to Co/Mo =1, followed by a steep decrease at a further incorporation of Co. The activity ratio, HYD/HDS, decreased as the Co content increased and reached the value for CoSx/NaY at the composition of the maximum HDS activity, as shown in Fig. 7. The product selectivity in the HYD of butadiene is presented in Fig. 8 for CoSx–MoSx/NaY. It is evident that the selectivity shifts from a *t*-2-butene-rich distribution to a 1-butene-rich composition on the addition of Co. It is noteworthy that, at the Co/Mo ratio of the maximum HDS activity, the butene distribution is close to that for CoSx/NaY. These results lead us to conclude that the HYD of butadiene

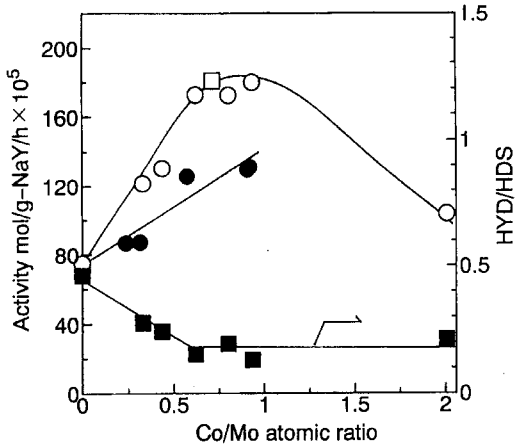


Fig. 7. HDS activity (○) and HYD/HDS activity ratio (■) of CoSx–MoSx/NaY (2.1Mo/SC) as a function of the Co/Mo atomic ratio. □; after a 20 h treatment in $H_2S/H_2$ at 673 K. The sum activities (●) of CoSx/NaY and MoSx/NaY are also shown for comparison.

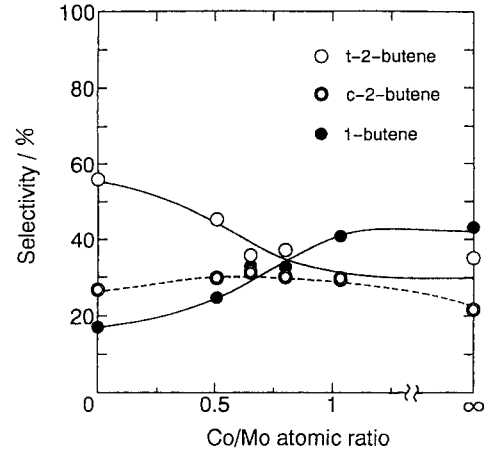


Fig. 8. Butene distribution of the HYD of butadiene over CoSx-MoSx/NaY (2.1Mo/SC) at 623 K as a function of the Co/Mo atomic ratio. ○, *t*-2-butene; , *cis*-2-butene and ●, 1-butene.

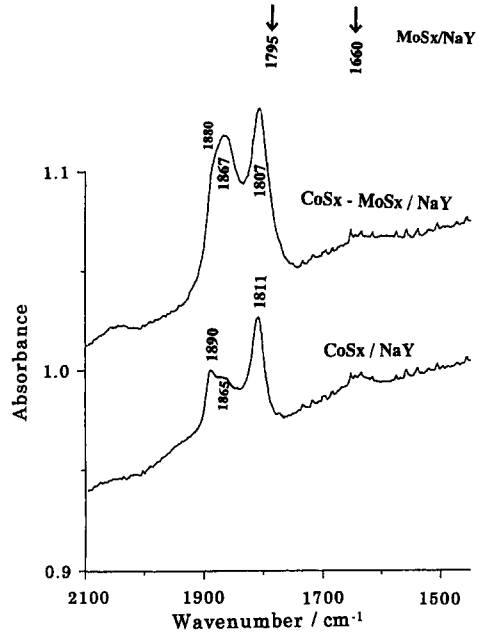


Fig. 9. FTIR spectra of NO adsorption on CoSx/NaY (2.1Co/SC) and CoSx–MoSx/NaY (2.1Co+2.1Mo/SC). Wave numbers for MoSx/NaY are indicated by arrows for comparison.

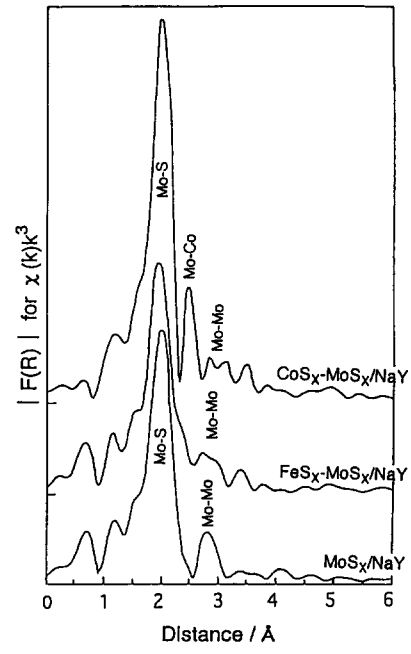


Fig. 10. $k^3$-weighted Fourier transforms of the Mo K-edge EXAFS for MoSx/NaY (2Mo/SC), FeSx–MoSx/NaY (Fe+2Mo/SC) and CoSx–MoSx/NaY (2Co+2Mo/SC).

takes place on the Co sites of the Co–Mo binary sulfide catalyst at Co/Mo=ca. 1 and that the Co sites play important roles in the HDS reaction, too.

Fig. 9 shows the FTIR spectra of NO adsorption on CoSx/NaY and CoSx–MoSx/NaY [39]. It is shown that NO molecules adsorb exclusively on Co sites, forming dinitrosyl species in spite of the presence of the equal amounts of Co and Mo atoms in the zeolite (2Co+2Mo/SC). The results in Fig. 9 clearly substantiate the proposition that the HYD of butadiene and, possibly, thiophene HDS proceed on the coordinatively unsaturated Co sites in the binary catalyst. The findings in Figs. 7–9 strongly suggest that Co–Mo mixed sulfides are formed in the zeolite pores rather than a physical mixture of highly dispersed Co and Mo sulfide clusters. On the basis of CO adsorption, Leglise et al. [41] proposed the formation of a Ni–Mo–S phase on USY-supported Ni–Mo catalysts prepared by a combination of ion-exchange and impregnation methods.

The formation of Co–Mo binary sulfides was studied by Mo K-edge EXAFS [39,52] and Co2p XPS [52] techniques. Fig. 10 shows the Fourier transform for CoSx–MoSx/NaY in comparison with that for MoSx/NaY. It is evident that a new Fourier transform peak appears in addition to the Mo–S and Mo–Mo bondings. The structural parameters as derived from the EXAFS analysis are presented in Table 1. The new peak was analyzed using theoretical parameters because of a lack of experimental EXAFS parameters for Co–Mo binary sulfide clusters. It was found that the peak appearing at 0.24 nm was reasonably curve-fitted ($R$ =10%) assuming only Mo–Co bondings [52]. This suggests that the peak is attributed to Mo–Co bondings and that the bond distance is 0.283 nm. The Mo–Co distance is close to that reported by Bouwens et al. for Co–Mo–S phases supported on activated carbon [57,58] and $SiO_2$ and $Al_2O_3$ [59]. At present, a lack of the experimental parameters for Mo–Co bondings restricts a further analysis (coordination number and more precise bond distance) of the EXAFS results.

The Co2p XPS spectra are presented in Fig. 11 for a variety of NaY-supported Co–Mo binary sulfide catalysts prepared using Mo and Co carbonyls [52]. CoSx–MoSx/NaY and MoSx–CoSx/NaY, in which $Co(CO)_3NO$ was used after and before Mo sulfide

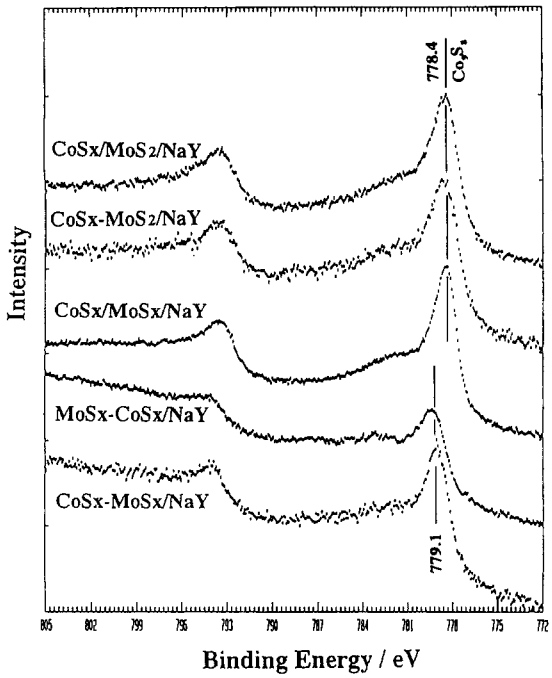


Fig. 11. Co2p XP spectra for CoSx–MoSx/NaY, MoSx–CoSx/NaY, CoSx/MoSx/NaY, CoSx–$MoS_2$/NaY and CoSx/$MoS_2$/NaY.

preparation, respectively, showed the $Co2p_{3/2}$ binding energy at 779.1 eV, the value being higher by 0.7 eV than that for $Co_9S_8$. Alstrup et al. [60] reported a similar size of the Co2p chemical shift for the Co sulfide species interacting with the edge sites of $MoS_2$. Accordingly, it is concluded that the XPS results for CoSx–MoSx/NaY and MoSx–CoSx/NaY substantiate the formation of Co–Mo binary sulfide clusters in conformity with the EXAFS results in Fig. 10. On the other hand, CoSx/MoSx/NaY prepared by use of $Co_2(CO)_8$ instead of $Co(CO)_3NO$ showed the $Co2p_{3/2}$ binding energy at 778.4 eV, indicating a formation of a $Co_9S_8$ phase on the surface of the sample. The higher binding energy of the Co2p level for the Co–Mo composite sulfides suggests an increased charge density on the Co sites by interactions with the Mo sulfide moiety.

Table 4 compares the XPS binding energies and intensity ratios for CoSx–MoSx/NaY and CoSx/MoSx/NaY catalysts [39]. The Co2p/Si2p XPS intensity ratio for the latter catalyst was much higher than that for the former system in spite of a lower Co content. These results disclose that a separate Co sulfide phase is formed on the external surface of $Co_2(CO)_8$-derived CoSx/MoSx/NaY. In the case of the Co–Mo catalysts based on $MoS_2$/NaY, a majority of surface Co species is present as $Co_9S_8$ because of an incomplete sulfidation and a poor dispersion of the Mo sulfide species.

As mentioned in Fig. 7, the thiophene HDS activity was maximized at the composition of Co/Mo=ca. 1. Taking into consideration the Mo content of 2Mo/SC, formations of highly dispersed Co–Mo binary sulfide clusters, possibly $Co_2Mo_2Sx$, in the supercage of the NaY zeolite are suggested for catalytically active species [39]. The composition of catalytically active Co–Mo binary sulfide species was estimated by means of XPS and XRF [52]. The compositions are summarized in Table 5. The XPS and XRF techniques provided the identical compositions. It should be noted that the former technique provides a surface composition (<5 nm), whereas the latter gives a bulk composition. Accordingly, it is concluded that the catalyst composition is homogeneous in depth. A clear Fourier

Table 4
XPS Results for Co–Mo binary sulfide catalysts

| Catalyst [a] | Binding energy (eV) [b] | | | Intensity ratio | |
|---|---|---|---|---|---|
| | $Co2P_{3/2}$ | $S2p_{3/2}$ | $Mo3d_{5/2}$ | Co2p/Si2p | Mo3d/Si2p |
| CoSx–MoSx/NaY(2.2) | 779.1 | 161.9 | 228.9 | 1.21 | 0.77 |
| CoSx–MoSx/NaY(1.2) | 778.4 | 161.9 | 228.9 | 2.62 | 0.85 |
| $Co_9S_8$ [c] | 778.4 | 162.1 [d] | — | — | — |

[a] Mo content, 2.1–2.2 atoms/SC. The number in parentheses denotes Co atoms/SC.
[b] Referenced to the Si2p level at 103.0 eV for the NaY zeolite.
[c] Alstrup et al., J Catal., 77(1982)397.
[d] $S2p_{1/2}$ + $S2p_{3/2}$.

Table 5
Composition of intrazeolite metal sulfides

| Metal sulfide | Loading/SC | | Composition | Technique |
|---|---|---|---|---|
| | Mo | Co or Fe | | |
| MoSx/NaY | 2.0 | | $MoS_{1.9-2.0}$ | XPS |
| | 1.9 | | $MoS_{2.1}$ | XRF |
| $MoS_2$/NaY [b] | 2.4 | | $MoS_{1.1}$ | XPS |
| CoSx/NaY | | 2.1 | $CoS_{1.0}$ | XRF |
| FeSx/NaY | | 2.1 | $FeS_{1.2}$ | XRF |
| CoSx–MoSx/NaY | 2.0 [a] | 2.0 [a] | $Co_{2.0}Mo_{2.0}S_{5.8}$ | XPS |
| | 1.9 | 2.0 | $Co_{2.0}Mo_{1.9}S_{5.7}$ | XRF |

[a] Chemical analysis using ICP and AAS; accuracy, ±0.1/SC.
[b] Prepared by an impregnation method.

transform peak due to the Mo–Co bondings in Fig. 10 also suggests a homogeneity of the structure of Co–Mo composite sulfide clusters in CoSx–MoSx/NaY (2Co+2Mo/SC). Consequently, it is proposed that $Co_2Mo_2S_6$ molecular clusters are formed in each supercage of the NaY host zeolite by means of the metal carbonyl techniques using $Mo(CO)_6$ and $Co(CO)_3NO$. As shown above, the hydrogenation and, possibly, HDS reactions take place on the Co sites of the $Co_2Mo_2S_6$ clusters. The structure of the intrazeolite $Co_2Mo_2S_6$ clusters is under investigation now but may be suggested to be a distorted cubane type structure. It has been shown [61,62] that in a homogeneous system, Mo sulfide dimer clusters react with $Co_2(CO)_8$ to form $Co_2Mo_2$ binary sulfide clusters with cubane structures.

In contrast to CoSx–MoSx/NaY, FeSx–MoSx/NaY, which was prepared by use of $Fe(CO)_5$, showed no catalytic synergies between Fe and Mo sulfides and the HDS activity of MoSx/NaY decreased upon the addition of Fe [52]. The Fourier transform for FeSx–MoSx/NaY showed no indication of Mo–Fe direct bondings as illustrated in Fig. 10. The Fe sulfides, which are catalytically inactive as shown in Fig. 4, are deduced to physically block the pre-existing Mo sulfide species in the zeolite cavities.

## 5. Mechanism of the catalytic synergy generation between Co and Mo sulfides

The mechanism of synergy generation or mutual promotive effects in Co–Mo binary sulfide catalysts has been extensively studied for HDS but still remains controversial at present [3,50,63–69]. Two major synergy models are under discussion now: a CoMoS model [63,64] and a contact synergy model [67]. In the CoMoS model, the formation of atomically dispersed Co sulfide species anchored on the edge sites of $MoS_2$ is claimed to be the origin of the synergy generation. In the contact synergy model, the promotional effects of Co are explained in terms of spillover hydrogen and thereby reconstructed $MoS_2$ edge sites (remote control theory). These models are schematically illustrated in Fig. 12 [50,69]. CoSx–MoSx/NaY is considered to represent the CoMoS model where $Co_2Mo_2S_6$ clusters are formed and Co–S–Mo chemical bondings are generated. On the other hand, CoSx/MoSx/NaY is conjectured to represent the contact synergy model, in which a considerable proportion of Co sulfide species are separately present outside the zeolite particles, but very closely located to the Mo sulfide species inside the pores.

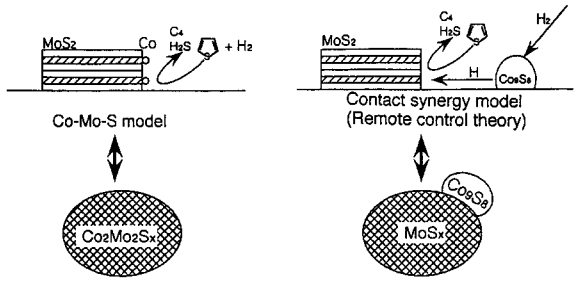


Fig. 12. Catalytic synergy generation in Co–Mo sulfide catalyst.

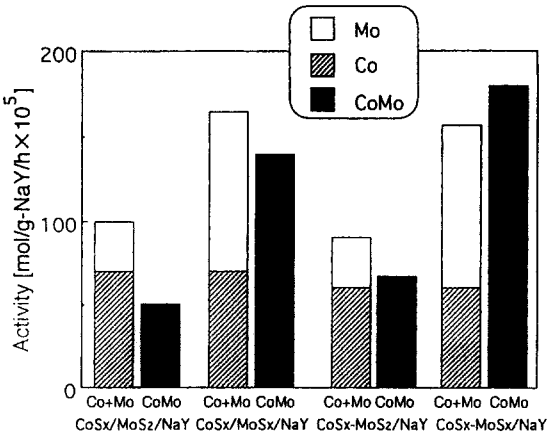


Fig. 13. HDS activities of the Co–Mo binary sulfide catalysts supported on NaY as compared to the sum activities of MoSx/NaY or $MoS_2$/NaY and CoSx/NaY.

The HDS activities of CoSx–MoSx/NaY and CoSx/MoSx/NaY are compared in Fig. 13 [50] with the sum activities of the corresponding CoSx/NaY and MoSx/NaY. CoSx–MoSx/NaY showed a greater HDS activity than the sum activity, while CoSx/MoSx/NaY exhibited almost the same activity as the sum activity. It is concluded that the formation of Co–Mo mixed sulfides are required for the synergy generation. In the case of $MoS_2$/NaY-based catalysts, no indication of synergy generation was observed as presented in Fig. 13. This may be explained in terms of the poor dispersion of Mo sulfide species and thereby a predominant production of $Co_9S_8$ as revealed by the XPS results in Fig. 11.

The formation of Co–Mo binary sulfide clusters in the NaY zeolite makes the Co sites coordinatively unsaturated while the Mo sites saturated, as directly evidenced by the FTIR spectra of NO adsorption in Fig. 9. The HYD/HDS activity ratio and the selectivity of butadiene HYD in Fig. 7 and Fig. 8, respectively, support the above findings, as discussed above. These results cannot be explained simply in terms of a physical blockage of the Mo sites by Co phases, since the accommodation order of Co and Mo into zeolite cages did not affect the HDS activity. It is proposed that the formation of highly, coordinatively unsaturated Co species results from a specific local structure of the Co atoms imposed by the formation of Co–Mo binary sulfide species. In the case of Co(Ni)–Mo–S phases, XANES and EXAFS studies indicated the formation of Co(Ni) species binding to four sulfur atoms on the edge sites of $MoS_2$ [57–59,70,71]. Cubane-type $Co_2Mo_2$ binary sulfide clusters, a proposed structure for $Co_2Mo_2S_6$ clusters, would provide Co species possessing three sulfur atoms and three vacant sites. HYD of butadiene has been proposed to take place on triply, coordinatively unsaturated metal sulfide sites [72].

The high coordinative unsaturation of the Co sites, however, does not necessarily mean weak Co-reactant interactions. Conversely, on the basis of the increased Co2p binding energies observed for the Co–Mo binary sulfide systems [39,52,60], it is conjectured that the adsorption strength of a reactant, such as thiophene, butadiene etc., on the Co sites in the Co–Mo binary sulfide clusters increases as compared to that on Co sulfide clusters because of increased charges on the Co sites. Harris et al. [73] proposed a charge transfer from Co to Mo atoms for a Co–Mo binary sulfide cluster model on the basis of SCF-X $\alpha$ calculations. An increase in the adsorption strength facilitates a nucleophilic attack of, for instance, thiophene on the Co sites, thereby strongly enhancing the HDS of thiophene per Co sites. In the case of desulfurization of thiols and thiophene using $Cp'_2\ Mo_2Co_2S_3(CO)_4$ (Cp′: methylpentadiene), it was revealed by Riaz et al. [74] that the desulfurization reaction was initiated by a nucleophilic attack of the sulfur compound on the Co sites of the bimetallic sulfide cluster but not on the Mo sites. This is nicely consistent with the catalytic properties of $Co_2Mo_2S_6$ clusters encapsulated in the NaY zeolite cavities. Very recently, on the basis of Bond Energy Model (BEM), Topsøe et al. [3,75] have proposed a possible reaction mechanism of HDS over a Co–Mo–S phase, in which mechanism a sulfur compound adsorbed on the Co sites is attacked by hydrogen atoms dissociated on the nearby Mo–S sites. The present results and propositions are in conformity with their mechanism. The local structures and electronics states of Co and Mo in $Co_2Mo_2S_6$ clusters are considered to be close to those for the Co–Mo–S phases [63,64,66,70,71]. However, different arrangements and combinations of the Co and Mo sites between these catalyst systems might induce different catalytic properties for HDS and HYD reactions. A further study on this subject is under way.

## 6. Concluding remarks

Preparation, characterization and catalytic properties of zeolite-supported Mo, Co(Ni) and Co(Ni)–Mo sulfide catalysts have been reviewed above. The conventional impregnation techniques led to incomplete sulfidation, poor dispersion of the resultant Mo sulfides and a partial destruction of the zeolite. Zeolite-supported Mo sulfide catalysts were also prepared by an ion-exchange technique using $MoO_2^{2+}$ or by a solid–solid reaction between $MoCl_5$ and zeolitic hydroxyl groups. These preparations provided catalysts similar to the impregnation catalysts. Highly dispersed and thermally stable intrazeolite Mo and Co sulfides were fabricated by metal carbonyl techniques. These catalysts exhibited much higher HDS activities than the impregnation catalysts. The metal carbonyl technique provided the way to synthesize intrazeolite Co–Mo binary sulfide clusters, possibly $Co_2Mo_2S_6$ molecular clusters. These clusters showed catalytic synergy for HDS. The Co sites were found to play important roles in HYD and HDS.

The aforementioned results suggest that combinations of hydroxyl groups and highly dispersed Co–Mo sulfides provide highly active hydrocracking catalysts. However, only a few studies have been conducted to clarify the mutual cooperations of two functions [76]. According to Hattori [77], with $Pt/SO_4^{2-}/ZrO_2$ catalysts, Pt metal generates new protonic sites on the support via hydrogen spillover with an electron being transferred to the support. Sachtler et al. [78] have proposed that the formation of Pd metal-$H^+$ adducts, $[Pd_nH_m]^{m+}$, in Pd/HY zeolite results in high catalytic performances for hydroisomerization reactions. Metal sulfides encaged in acidic zeolite would provide similar synergistic effects. Recently, Welters et al. [79] suggested a synergy between Ni sulfides and acidic sites for thiophene HDS on Ni/HY catalysts.

## Acknowledgements

This work has been carried out as a research project of The Japan Petroleum Institute commissioned by the Petroleum Energy Center with the subsidy of the Ministry of International Trade and Industry. This work was also supported by a Grand-in-Aid for Scientific Research on Priority Area "Catalytic Chemistry of Unique Reaction Field" (No. 08232251) from the Ministry of Education, Science, Sport and Culture. The X-ray absorption experiments at the Mo and Co K-edges were performed under the approval of the Photon Factory Program Advisory Committee (Proposal No. 90150, 92018 and 93G163).

## References

[1] I.E. Maxwell, Catal. Today 1 (1987) 385.
[2] M. Bryssee, J.L. Portefaix, M. Vrinat, Catal. Today 10 (1991) 489.
[3] H. Topsøe, B.S. Clausen, F.E. Massoth, in: J.R. Anderson, M. Boudard (Eds.), Catalysis-Science and Technology, Vol. 11, Springer, Berlin, 1996, p. 1.
[4] A. Lopez Agudo, R. Cid, F. Orellana, J.L.G. Fierro, Polyhedron 5 (1986) 187.
[5] R. Cid, F.J. Gil Llambias, J.L.G. Fierro, A. Lopez Agudo, J. Villasenor, J. Catal. 89 (1984) 478.
[6] R. Cid, F. Orellana, A. Lopez Agudo, Appl. Catal. 32 (1987) 327.
[7] J.L.G. Fierro, J.C. Conesa, A. Lopez Agudo, J. Catal. 108 (1987) 334.
[8] J. Thoret, C. Marchal, C. Doremieux-Morin, P.P. Man, M. Gruia, J. Fraissard, Zeolites 13 (1993) 269.
[9] J.A. Anderson, B. Pawelec, J.L.G. Fierro, Appl. Catal. A 99 (1993) 37.
[10] A. Lopez Agudo, A. Benitez, J.L.G. Fierro, J.M. Palacios, J. Neira, R. Cid, J. Chem. Soc. Faraday Trans. 88 (1992) 385.
[11] A. Corma, M.I. Vazquez, A. Bianconi, A. Clozza, J. Garcia, O. Pollota, J.K. Cruz, Zeolites 8 (1988) 464.
[12] Y. Okamoto, H. Katsuyama, Ind. Eng. Chem. Res. 35 (1996) 1834.
[13] G. Vorbeck, W.J.J. Welters, L.J.M. van de Ven, H.W. Zandbergen, J.W. de Haan, V.H.J. de Beer, R.A. van Santen, Zeolites and Related Microporous Materials: State of the Art, 1994, Elsevier, Amsterdam, 1994, p. 1617.
[14] A.V. Kucherov, A.A. Slinkin, Zeolites 7 (1987) 38.
[15] M. Huan, J. Yao, S. Xu, Ch. Meng, Zeolites 12 (1992) 810.
[16] J. Cui, Y. Yue, Y. Sun, W. Dong, Z. Cao, Proc. 11th International Zeolite Conference, 1996, Seoul, paper OA35.
[17] S.D. Djajanti, R.F. Howe, Proc. 11th International Zeolite Conference, 1996, Seoul, paper PP20.
[18] A. Corma, A. Martinez, V. Martinez-Soria, J.B. Monton, J. Catal. 153 (1995) 25.
[19] E.L. Moorehead, US Patent, 4,297,243, 1981.
[20] H. Minming, R.F. Howe, J. Catal. 108 (1987) 283.
[21] A. Ezzamarty, E. Catherine, D. Cornet, J.F. Hemidy, A. Janin, J.C. Lavalley, J. Leglise, in: P.A. Jacobs, R.A. van Santen (Eds.), Zeolites: Facts, Figures, Futute, Elsevier, Amsterdam, 1989, p. 1025.
[22] P.-S.E. Dai, J.H. Lunsford, J. Catal. 64 (1980) 173.

[23] P.-S.E. Dai, J.H. Lunsford, J. Catal. 64 (1980) 184.
[24] J.R. Johns, R.F. Howe, Zeolites 5 (1985) 252.
[25] M.T. Oluguin, P. Bosch, J.M. Dominguez, S. Bulbulian, Zeolites 13 (1993) 494.
[26] R.F. Howe, J. Ming, W. She-Tin, Z. Jian-Hua, Catal. Today 6 (1989) 113.
[27] T. Komatsu, S. Namba, T. Yashima, K. Domen, T. Onishi, J. Mol. Catal. 33 (1985) 345.
[28] R.F. Howe, in: Y. Iwasawa (Ed.), Tailored Metal Catalysts, Reidel, Dordrecht, 1986, p. 141.
[29] Y. Yong-Sing, R.F. Howe, J. Chem. Soc., Faraday Trans. 1(82) (1986) 2887.
[30] Y. Okamoto, A. Maezawa, H. Kane, T. Imanaka, in: M.J. Phillips, M. Ternan (Eds.), Proceedings 9th International Congress on Catalysis, Vol. 1, The Chemical Institute of Canada, Ottawa, 1988, p. 11.
[31] Y. Okamoto, A. Maezawa, H. Kane, T. Imanaka, J. Mol. Catal. 52 (1989) 337.
[32] M. Laniecki, W. Zmierczak, Zeolites 11 (1991) 18.
[33] M. Laniecki, W. Zmierczak, in: C.H. Batholomew, J.B. But (Eds.), Catalyst Deactivation, Elsevier, Amsterdam, 1991, p. 799.
[34] M.L. Vrinat, C.G. Gachet, L.de Mourgues, in: B. Imelik et al. (Eds.), Catalysis by Zeolites, Elsevier, Amsterdam, 1980, p. 219.
[35] M. Laniecki, W. Zmierczak, in: P.A.Jacobs et al. (Eds.), Zeolite Chemistry and Catalysis, Elsevier, Amsterdam, 1991, p. 331.
[36] R. Jelinek, S. Özkar, G.A. Ozin, J. Phys. Chem. 96 (1992) 5949.
[37] Y. Okamoto, Y. Kobayashi, T. Imanaka, Catal. Lett. 20 (1993) 49.
[38] S. Abdo, R.F. Howe, J. Phys. Chem. 87 (1983) 1722.
[39] Y. Okamoto, H. Katsuyama, Shokubai (Catalyst) 37 (1995) 144; Y. Okamoto, H. Katsuyama, in: J.W. Hightower, W.N. Delgass, E. Iglesia (Eds.), 11th International Congress on Catalysis - 40th Anniversary, Vol. 1, Elsevier, Amsterdam, 1996, p. 503.
[40] G.-C. Shen, T. Shido, M. Ichikawa, J. Phys. Chem. 100 (1996) 16947.
[41] J. Leglise, A. Janin, J.C. Lavalley, D. Cornet, J. Catal. 114 (1988) 388.
[42] J.A. Anderson, B. Pawelec, J.L.G. Fierro, P.L. Arias, F. Duque, J.F. Cambra, Appl. Catal. A 99 (1993) 55.
[43] Y. Okamoto, H. Katsuyama, K. Yoshida, K. Nakai, M. Matsuo, Y. Sakamoto, J. Yu, O. Terasaki, J. Chem. Soc. Faraday Trans. 92 (1996) 4647.
[44] W.J.J. Welters, G. Vorbeck, H.M. Zandbergen, J.W. de Haan, V.H.J. de Beer, R.A. van Santen, J. Catal. 150 (1994) 155.
[45] R. Cid, J. Villasenor, F. Orellana, J.L.G. Fierro, A. Lopez Agudo, Appl. Catal. 18 (1985) 357.
[46] N. Herron, Y. Wang, M.M. Eddy, G.D. Stucky, D.E. Cox, K. Moller, T. Bein, J. Am. Chem. Soc. 111 (1989) 530.
[47] H. Taniguchi, S. Yasuda, Y. Ishii, T. Murata, M. Hidai, T. Tatsumi, in: J.W. Hightower, W.N. Delgass, E. Iglesia (Eds.), 11th International Congress on Catalysis - 40th Anniversary, Vol. 1, Elsevier, Amsterdam, 1996, p. 107.
[48] T.R. Halbert, T.C. Ho, E.I. Stiefel, R.R. Chianelli, M. Daage, J. Catal. 130 (1991) 116.
[49] Y. Okamoto, M. Odawara, H. Onimatsu, T. Imanaka, Ind. Eng. Chem. Res. 34 (1995) 3703.
[50] Y. Okamoto, in: M. Absi-Halabi et al. (Eds.), Catalysts in Petroleum Refining and Petrochemical Industries, 1995, Elsevier, Amsterdam, 1996, p. 77.
[51] Y. Okamoto, A. Maezawa, H. Kane, I. Mitsushima, T. Imanaka, J. Chem. Soc., Faraday Trans. 1(84) (1988) 851.
[52] Y. Okamoto, H. Katsuyama, Preprint of 5th World Congress on Chemical Engineerings, Vol. IV, San Diego, 1996, p. 651; Y. Okamoto, H. Katsuyama, AIChE J., in press.
[53] Y. Sakamoto, N. Togashi, O. Terasaki, T. Ohsuna, Y. Okamoto, K. Hiraga, Material Sci. Eng. 217/218 (1996)147.
[54] M. Zdrazil, Collect. Czech. Chem. Commun. 40 (1975) 3491.
[55] M. Zdrazil, Collect. Czech. Chem. Commun. 42 (1977) 1484.
[56] J.P.R. Vissers, V.H.J. de Beer, R. Prins, J. Chem. Soc., Faraday Trans. 1(83) (1987) 2145.
[57] S.M.A.M. Bouwens, R. Prins, H.H.J. de Beer, D.C. Koningsberger, J. Phys. Chem. 94 (1990) 3711.
[58] S.M.A.M. Bouwens, J.A.R. van Veen, D.C. Koningsberger, V.H.J. de Beer, R. Prins, J. Phys. Chem. 95 (1991) 123.
[59] S.M.A.M. Bouwens, F.B.M. van Zon, M.P. van Dijk, A.M. van der Kraan, V.H.J. de Beer, J.A.R. van Veen, D.C. Koningsberger, J. Catal. 146 (1994) 375.
[60] I. Alstrup, I. Chorkendorff, R. Candia, B.S. Clausen, H. Topsøe, J. Catal. 77 (1982) 397.
[61] T.R. Halbert, S.A. Cohen, E.I. Stiefel, Organometallics 4 (1985) 1689.
[62] E.I. Stiefel, T.R. Halbert, C.L. Coyle, L. Wei, W.-H. Pan, T.C. Ho, R.R. Chianelli, M. Daage, Polyhedron 8 (1989) 1625.
[63] H. Topsøe, B.S. Clausen, Catal. Rev. -Sci. Eng. 26 (1984) 395.
[64] H. Topsøe, B.S. Clausen, N.-Y. Topsøe, E. Pederson, Ind. Eng. Chem. Fundam. 25 (1986) 25.
[65] R.D. Chianelli, Catal. Rev. -Sci. Eng. 26 (1984) 361.
[66] R. Prins, V.H.J. de Beer, G.A. Somorjai, Catal. Rev. -Sci. Eng. 31 (1989) 1.
[67] B. Delmon, Catal. Lett. 22 (1993) 1.
[68] R.R. Chianelli, M. Daage, M.J. Ledoux, Adv. Catal. 40 (1994) 177.
[69] Y. Okamoto, Shokubai (Catalyst) 38 (1996) 26; Y. Okamoto Petrotech, 20 (1997) 389.
[70] W. Niemann, B.S. Clausen, H. Topsøe, Catal. Lett. 4 (1990) 355.
[71] S.P.A. Louwens, R. Prins, J. Catal. 133 (1992) 94.
[72] K. Tanaka, T. Okuhara, Catal. Rev. -Sci. Eng. 15 (1977) 249.
[73] S. Harris, R.R. Chianelli, J. Catal. 98 (1986) 17.
[74] U. Riaz, O.J. Curnow, M.D. Curtis, J. Am. Chem. Soc. 116 (1994) 4357.
[75] H. Topsøe, B.S. Clausen, N.-Y. Topsøe, J.K. Norskov, C.V. Ovesen, C.J.H. Jacobsen, Bull. Soc. Chim. Belg. 104 (1995) 283.
[76] W.C. Conner, J.L. Falconer, Chem. Rev. 95 (1995) 759.
[77] H. Hattori, in: T. Inui, K. Fujimoto, T. Uchijima, M. Masai (Eds.), Stud. Surf. Sci. Catal., Elsevier, Amsterdam, 1993, p. 69.
[78] W.M.H. Sachtler, A.Yu. Stakheev, Catal. Today 12 (1992) 283.
[79] W.J.J. Welters, V.H.J. de Beer, R.A. van Santen, Appl. Catal. A 119 (1994) 253.